

# Pendular-state spectroscopy of the $S_1-S_0$ electronic transition of 9-cyanoanthracene

Reika Kanya and Yasuhiro Ohshima<sup>a)</sup>

*Department of Chemistry, Graduate School of Science, Kyoto University, Kitashirakawa-Oiwakecho, Sakyo-ku, Kyoto 606-8502, Japan*

(Received 3 June 2004; accepted 23 August 2004)

Fluorescence excitation spectra of the  $S_1-S_0$  origin band of 9-cyanoanthracene have been observed under a uniform electric field up to 200 kV/cm to explore pendular-state spectrum of an asymmetric-top molecule close to the strong field limit. The observed spectra exhibit distinct evolution of the band contour as a function of the applied electric field, which are much different from each other for different excitation configurations. An approximate method suitable for spectrum simulations of large asymmetric-top molecules in a pendular condition is developed for the analysis of the experimental results. The comparison of the observed and simulated spectra shows that the spectra are well ascribed in terms of the pendular-state selection rules, which have recently been derived from theoretical consideration of the pendular-limit representation of energy levels and spectra [R. Kanya and Y. Ohshima, *Phys. Rev. A* **70**, 013403 (2004)]. © 2004 American Institute of Physics. [DOI: 10.1063/1.1806420]

## I. INTRODUCTION

When a polar molecule is in a dc electric field, the molecule tends to orient its dipole to the electric field. If the dipole-field interaction overcomes the rotational energy, the molecule cannot rotate freely but librates around the field axis, and the orientation of the molecule is confined in the laboratory frame. In 1990, Loesch and Remscheid<sup>1</sup> realized such a laboratory-frame orientation by applying a strong dc electric field with the combination of a rotational cooling by a supersonic expansion and utilized the technique to investigate a steric effect in reactive collisions. Independently, in 1991, Friedrich and Herschbach<sup>2</sup> started spectroscopic studies of polar molecules in a strong electric field. They named the state confined in the dipole-field interaction potential “pendular state.” Thereafter, pendular states have been frequently explored in various studies for spectroscopies,<sup>3</sup> steric effects of reactions,<sup>4</sup> controls of molecular orientation<sup>5–12</sup> and tunneling motions,<sup>13</sup> photodissociation dynamics of molecules<sup>14</sup> and complexes,<sup>15–17</sup> measurements of electric-dipole moments,<sup>18–21</sup> determinations of transition-dipole orientations,<sup>22–24</sup> and superfluid helium droplet spectroscopies.<sup>25–29</sup>

Among the previous studies mentioned earlier, the experimental application to an asymmetric-top molecule and the corresponding theoretical consideration were reported by Moore *et al.*, who observed infrared spectra of the near prolate acetylene-HF complex.<sup>3</sup> Kong and co-workers extensively applied pendular-state spectroscopy to aromatic molecules.<sup>8,10,11,23,24</sup> A theoretical study on the orientation of asymmetric tops was also reported.<sup>7</sup> These studies have shown that energy levels and spectra of pendular-state asymmetric-top molecules are much more complicated than

those of linear or symmetric-top molecules. Numerical calculations have been carried out by the direct diagonalization of a Hamiltonian matrix constructed with the free-rotation basis set, and energy levels, wave functions, and spectra have been accurately derived as long as the size of the basis set is sufficient.<sup>3,7,8,10,11</sup> One of the drawbacks of the diagonalization method is that gross features of energy levels and spectral pattern cannot be interpreted until detailed inspection of the numerical outputs, because the resultant wave functions are represented by highly mixed linear combinations of the free-rotation bases.

Quite recently, we examined pendular-limit representation of energy levels and spectra of asymmetric-top as well as symmetric-top molecules by an appropriate coordinate transformation and a power-series expansion.<sup>30</sup> It has been shown that motions of asymmetric tops in a high field are well described as two-dimensional anisotropic harmonic oscillations, and pendular-state quantum numbers have been introduced to label the energy levels. Energies are analytically represented with the quantum numbers, and selection rules are derived with the consideration of symmetry groups appropriate to molecules in an external field. Transition strengths are evaluated also analytically for all the excitation configurations with each of the transition types. These results should provide a clear-cut description of the spectra of asymmetric tops in a high-field condition, yet to be evaluated by the comparison with experimental observations.

The evaluation of the pendular-limit representation demands that the electric field is as high as possible. The serious problem to realize this is that an electric discharge may take place at the electrodes to apply the high voltages. Among the previous studies, to our best knowledge, only two groups have succeeded in applying electric fields exceeding 100 kV/cm. Bemish *et al.* measured optothermal infrared spectra of HF dimer in a uniform electric field at 0–150

<sup>a)</sup>Present address: Institute for Molecular Science, Okazaki, 444-8585, Japan. Electronic mail: ohshima@kuchem.kyoto-u.ac.jp

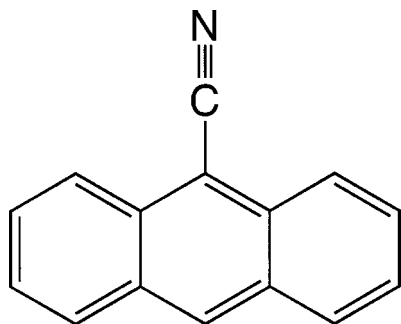


FIG. 1. Structure of 9-cyanoanthracene (9CNA).

kV/cm and observed a quenching of the tunneling motion that is characteristic to the HF dimer.<sup>13</sup> Hese and co-workers reported several measurements of high-resolution Stark spectroscopy by using an apparatus that realizes a uniform electric field up to 300 kV/cm.<sup>31–34</sup> We have recently constructed an apparatus that is capable of applying a uniform field up to 200 kV/cm, with a pair of electrodes specially designed to prevent the electric discharge, and utilized it to the determination of the dipole-moment change in the electronic excitation of Coumarin 153.<sup>21</sup> The present paper represents full descriptions of the experimental setup.

Here, we report fluorescence excitation spectra of 9-cyanoanthracene (9CNA), see Fig. 1, measured in a uniform electric field with various field strength up to 200 kV/cm. 9CNA has been chosen because of several suitable properties for exploring the pendular-state spectrum of an asymmetric-top molecule close to the strong field limit. First, its molecular parameters to characterize the pendular-state spectrum are precisely known by our previous studies.<sup>35,36</sup> Rotational constants in the  $S_0$  and  $S_1$  states have been determined by rotational coherence spectroscopy,<sup>35</sup> and Fourier-transform microwave spectroscopy has been applied to determine the electric-dipole moment in  $S_0$  as well as to refine the  $S_0$  rotational constants.<sup>36</sup> Second, pendular-limit condition can be realized even at relatively weaker field strength owing to the small rotational constants and large dipole moment of 9CNA. Third, by virtue of its symmetry, the permanent dipole moment points along one of the principal axes (i.e.,  $b$  axis), which makes spectral analyses simpler and effects of asymmetry in the pendular-state spectrum most pronounced.<sup>30</sup> Fourth, the fluorescence quantum yield of the  $S_1$ – $S_0$  origin band is almost unity,<sup>37</sup> and thus 9CNA is suitable for fluorescence excitation measurements. In addition, effects of nonradiative dynamics need not to be considered in analyses of obtained spectra.

The present paper is organized as follows. First, we depict the newly constructed apparatus that enables measurements of laser-induced fluorescence (LIF) in a strong electric field in Sec. II. In Sec. III, a detailed description is given on an approximate method, which is applicable for the calculation of energy levels and spectra of large asymmetric-top molecules in a pendular condition. Because the method is in accordance with the theoretical considerations by the pendular-limit formalism developed in Ref. 30, the required computation is particularly reduced from the direct diagonalization method and the utilities of the state assignments and

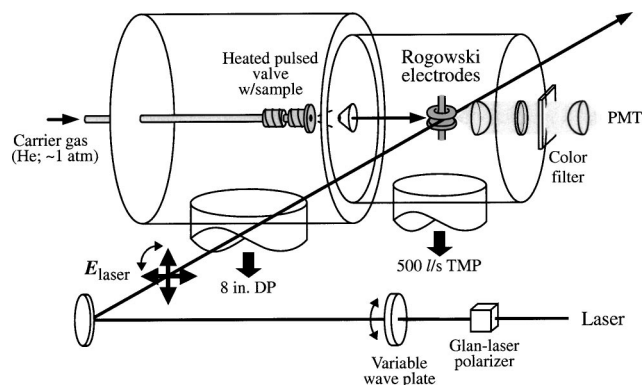


FIG. 2. Experimental setup.

selection rules are fully implemented. For spectrum simulations, the distribution of the ground-state population should be evaluated. In this paper, a population transfer model is presented to estimate the evolution of the thermally distributed population in the field-free condition to the pendular states under a uniform electric field. Section IV describes the results and discussion on the fluorescence excitation spectra of 9CNA recorded in the pendular condition. The observed spectra are analyzed by the comparison with the spectral simulations based on the method presented in Sec. III, and characteristics of the spectra recorded in the different excitation configurations are discussed to show the versatility in transition assignments by pendular-state selection rules.

## II. EXPERIMENT

The experimental setup for measurements of fluorescence excitation spectra in a strong dc electric field is schematically shown in Fig. 2. The apparatus consists of differentially pumped two vacuum chambers, divided by a conical skimmer. The first chamber is evacuated by an 8-in. diffusion pump, which is backed by a mechanical booster pump and a rotary pump. The second chamber is pumped by a molecular turbo pump (500 l/s) backed by a rotary pump.

Purchased 9CNA was used without further purifications. 9CNA was contained in a sample reservoir, which was directly attached to the nozzle. In order to gain a sufficient vapor pressure of the sample, both the reservoir and the nozzle were heated to around 150 °C by a sheath heater surrounding them. The sample vapor was entrained in a helium carrier gas and expanded into the first chamber through a pulsed solenoid valve (General Valve) with an 800- $\mu$ m-diameter orifice. A sufficiently cooled sample was generated by the supersonic expansion with a 3.0-atm stagnation pressure. The supersonic free jet was collimated by the 1.0-mm-diameter orifice of the skimmer set at 30 mm downstream from the nozzle. The resultant molecular beam was introduced into the second chamber. The pressure was maintained at  $1.0 \times 10^{-3}$  Pa in the first chamber during the experiments.

In the second chamber, two parallel electrodes are mounted at 200 mm downstream from the top of the skimmer. The shape of these electrodes is so-called of Rogowski type. Figure 3(a) illustrates the electric field around the Rogowski-type electrodes, in which the thin lines represent contours of the electric-field strength. In Fig. 3(b), the field

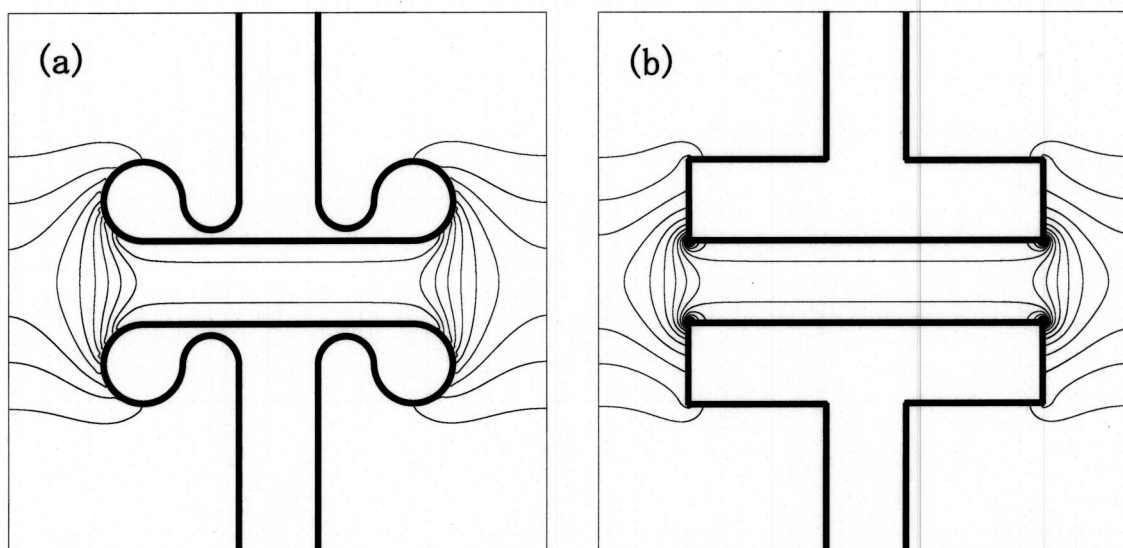


FIG. 3. Electric fields around (a) the Rogowski-type electrodes and (b) flat electrodes with a similar size. Thin lines represent contours of the electric-field strength. Both types of the electrodes are cylindrical, and their cross sections are shown.

around flat electrodes with the similar size is presented for the sake of comparison: points with extraordinary strong fields exist at the edges of the electrodes and electric discharges tend to occur at these points. Rogowski-type electrodes are designed to make an electric field change as smooth as possible even at the edges of the electrodes, as shown in Fig. 3(a). In our case, the diameter of the electrodes is 13.0 mm, whose edge is rounded with a radius of 1.5 mm, and the distance between them is 3.0 mm. The electrodes are made of an electrolytic polished stainless steel and held by a mount made of machinable ceramics. Cables are connected to the electrodes at the outside of the mount. Positive and negative high voltages up to 30 kV can be applied to each of the electrodes. Then, electric-field strengths up to 200 kV/cm are available while electric discharges seldom take place. Since their flatness and absolute spacing were estimated to be better than 0.1 mm, errors of the field accuracy and uniformity were within  $\pm 3\%$ . For the purpose of further collimation of the molecular beam, an aperture of 3.0-mm diameter was placed on the mount at 25 mm upstream from the center of the electrodes. The pressure of the second chamber was kept at  $4.0 \times 10^{-4}$  Pa. A pair of high-voltage power supplies of opposite polarities (Matsusada HSL-30P and -30N) were assembled, whose maximum voltages were  $\pm 30$  kV. Thus, the maximum electric-field strength was limited solely by the power supplies.

The source of excitation laser light is a XeCl excimer-laser (Lambda Physik LPX100) pumped dye laser (Lambda Physik LPD3000). An UV light of 375–385 nm was generated using a BBQ dye (Lambda Physik). The frequency resolution of the dye laser was  $0.2 \text{ cm}^{-1}$ . A Glan-laser polarizer was used to improve the polarization ratio of the linearly polarized laser light. The polarization plane of the light was rotated by a variable wave plate (used as a half-wave plate in this case) in order to make it parallel or perpendicular to the dc electric field. The resultant light was collimated by a 1.0-mm-diameter aperture and concentrated on the center be-

tween the two electrodes by a spherical lens with  $f = 500$  mm. The excitation laser went across the molecular beam at right angles to both the beam and the electric field. Another aperture (1.0-mm diameter) was mounted 25 mm in front of the center of the electrodes in order to prevent the light from hitting the electrodes accidentally.

Sample molecules were irradiated at the center of the two electrodes, and the resultant fluorescence was collected by a lens (40-mm diameter,  $f = 50$  mm) mounted at 50 mm downstream of the molecular beam. The collected photons were filtered by a sharp-cut long-pass filter (Schott GG420), and only fluorescence  $> 420$  nm was imaged onto a photomultiplier tube by another lens. The detected signal was preamplified, sent to a boxcar integrator (SRS SR250), and stored in a personal computer. The laser power was also measured by a photodiode. In order to suppress the scatter from the surface of the electrodes, the excitation laser was considerably attenuated. Thus, saturation effects in the excitation spectra were negligible.

### III. APPROXIMATE METHOD FOR SPECTRUM SIMULATION OF ASYMMETRIC-TOP MOLECULES

#### A. Calculation of energy levels and transition strengths

A matrix diagonalization method is frequently adopted in simulations of pendular-state spectra. In this procedure, the Hamiltonian matrix is constructed with the field-free basis set for the wave functions of a symmetric top, and diagonalization of the matrix provides the energy levels and wave functions of the pendular states. This method is useful as long as only lower  $v_{x,y}$  states are considered, where  $v_x$  and  $v_y$  are quantum numbers for pendular vibration introduced in Ref. 30. In a case where the ground-state population is spread over higher  $v_{x,y}$  states, it becomes difficult to simulate spectra with this procedure. In the case of asymmetric tops, the Hamiltonian matrix cannot be represented as block

diagonal in  $k$ , a projection of a rotational angular momentum  $j$  onto the molecular principal axis. Then, the dimension of the Hamiltonian matrix becomes the order of  $(j_{\max})^2$ , where  $j_{\max}$  is the maximum  $j$  of the basis set. On the other hand, the corresponding dimension about a linear rotor or a symmetric top is in the order of  $(j_{\max})^1$ . As a result, the matrix diagonalization and the calculation of oscillator strength are extremely time consuming in comparison with the calculations for a linear rotor or a symmetric top. Especially, spectrum simulations of large asymmetric-top molecules with this procedure are impractical, because the basis set with large  $j_{\max}$  must be required to cover widely spread population distribution owing to the small rotational constants even in a supersonic expansion.

We introduce here an approximate method for simulating the pendular-state spectra of the asymmetric-top molecules. For simplicity, the permanent dipole-moment vector,  $\mu$ , is assumed to be parallel to one of the principal axes of inertia (denoted as  $z$  axis), as is the case of 9CNA. The full Hamiltonian of such a polar asymmetric-top molecule in a uniform electric field is expressed as

$$\begin{aligned}\hat{H} &= \sigma_x \hat{j}_x^2 + \sigma_y \hat{j}_y^2 + \sigma_z \hat{j}_z^2 - \frac{2}{\lambda^2} \cos \theta \\ &= \hat{j}^2 + (\sigma_z - 1) \hat{j}_z^2 + \frac{\sigma}{2} (\hat{j}_+^2 + \hat{j}_-^2) - \frac{2}{\lambda^2} \cos \theta,\end{aligned}\quad (1)$$

where  $\hat{j}_{\pm}$  are ladder operators of angular momentum in the molecular-fixed frame and  $\theta$  is the angle between the external field vector and the  $z$  axis. An energy is represented by a reduced unit of an average of rotational constants, and the coefficients appearing in Eq. (1) are represented as

$$\sigma_g = \frac{2B_g}{B_x + B_y}, \quad (2)$$

$$\sigma = (\sigma_x - \sigma_y)/2, \quad (3)$$

$$\lambda = \sqrt{\frac{B_x + B_y}{\mu \epsilon}}, \quad (4)$$

where  $B_g$  is the rotational constant around the  $g$  ( $=x, y, z$ ) axis and  $\epsilon$  is the external electric field. The parameter  $\lambda$  represents the degree of the pendular condition and approaches zero in the strong field limit. General cases where  $\mu$  points to none of the principal axes have been discussed in Ref. 30. Then, the full Hamiltonian is divided into two parts,  $\hat{H}_{\text{sym}}$  and  $\hat{H}_{\Delta k}$ ,

$$\hat{H}_{\text{sym}} = \hat{j}^2 + (\sigma_z - 1) \hat{j}_z^2 - \frac{2}{\lambda^2} \cos \theta, \quad (5)$$

$$\hat{H}_{\Delta k} = \frac{\sigma}{2} (\hat{j}_+^2 + \hat{j}_-^2). \quad (6)$$

Since  $\hat{H}_{\text{sym}}$  is identical to the full Hamiltonian of a polar symmetric-top molecule in a uniform electric field,  $k$  behaves as a good quantum number as long as  $\hat{H}_{\text{sym}}$  is only considered.  $\hat{H}_{\Delta k}$  manifests deviations from symmetric tops and acts as the  $k$ -mixing term.

Firstly, matrices of  $\hat{H}_{\text{sym}}$  on the free-rotation basis set,  $|j, k, m\rangle$ , are constructed analytically using integral formula of rotation matrices. Diagonalizations of the matrices yield energies and wave functions of  $\hat{H}_{\text{sym}}$ . Note that the dimension of the matrix is at most  $j_{\max} + 1$ . The resultant wave functions can be relabeled in terms of the pendular quantum numbers for symmetric tops,  $v$ ,  $l$ , and  $m$ , whose values are derived from the correlation to the free-rotation quantum numbers,<sup>30</sup> namely,

$$v = |l| + 2n, \quad (7)$$

$$l = m - k, \quad (8)$$

where  $n = 0, 1, 2, \dots$  is a numbering of eigenstates in increasing order of energy in a  $(|m|, |l|)^{\pm}$  matrix of  $\hat{H}_{\text{sym}}$ .  $(|m|, |l|)^{\pm}$  is a label for an irreducible representation defined in Ref. 30. Thus, a pendular wave function,  $|v, l, m\rangle$ , is represented by a linear combination of  $|j, k, m\rangle$ . Among the eigenstates of  $\hat{H}_{\text{sym}}$ , wave functions of  $v = 0, 1, 2, \dots, v_{\max}$  are selected as a pendular basis set, where  $v_{\max}$  is the maximum  $v$  in the basis set.

Next, matrices of  $\hat{H}_{\text{sym}} + \hat{H}_{\Delta k}$  are constructed by the basis set of  $|v, l, m\rangle$ . In this step, we consider only couplings between states with the same  $v$ . Although  $\hat{H}_{\Delta k}$  also mixes states with different  $v$ , the mixings between the same  $v$  states are far greater than those between the different  $v$ . Due to this approximation, dimensions of the matrices are at most  $v_{\max} + 1$ . After diagonalization of the matrices, energies and wave functions are obtained. Because the vibrational quantum numbers of two-dimensional anisotropic and isotropic harmonic oscillators satisfy the relation of  $v_x + v_y = v$ , the obtained wave functions can be relabeled in terms of  $v_x$ ,  $v_y$ , and  $m$  as follows: If  $\sigma_x > \sigma_y$ ,  $(v_x, v_y) = (i, v - i)$ , and if  $\sigma_x < \sigma_y$ ,  $(v_x, v_y) = (v - i, i)$ , where  $i = 0, 1, \dots, v$  is a numbering of eigenstates in increasing order of energy.

In order to calculate transition oscillator strengths, a matrix of  $\langle v', l', m' | \mu_{Fg} | v'', l'', m'' \rangle$  is firstly evaluated, where  $\mu_{Fg}$  is the component of the transition dipole operator for space-fixed  $F$  ( $=X, Y, Z$ ) and molecule-fixed  $g$  ( $=x, y, z$ ). Transition oscillator strengths between the  $|v_x, v_y, m\rangle$  wave functions can be evaluated with these matrix elements and the transformation matrix between  $|v, l, m\rangle$  and  $|v_x, v_y, m\rangle$ .

This method is an approximation, and some discrepancies arise in energy levels and spectra because of the neglect of the different  $v$  coupling by  $\hat{H}_{\Delta k}$ . However, the accuracy of this method is sufficient for analyses of spectra of large molecules, of which fine rotational structure can only be partly resolved in an ordinary experimental condition. The method has the following several advantages. The direct diagonalization method using the free-rotation basis set, which has been frequently adopted in the previous works, requires diagonalizations of matrices with dimensions of the  $(j_{\max})^2$  order. The matrix diagonalizations in the present method are separated into two steps, the generation of the pendular basis set  $|v, l, m\rangle$  and the final wave functions  $|v_x, v_y, m\rangle$ . The dimensions of the former matrices are at most  $j_{\max} + 1$ , and those of the latter are at most  $v_{\max} + 1$ . Therefore, required computational efforts can be substan-

tially reduced from the direct diagonalization method, where the matrices with dimensions of the  $(j_{\max})^2$  order have to be dealt with. Furthermore, the most valuable feature of this method is the ability of labeling states in terms of  $v_x$  and  $v_y$ . This allows us to utilize the theoretical results of the pendular-limit formalism presented in Ref. 30. For example, we can omit transitions with large  $\Delta v_{x,y}$  in calculations of transition strengths because these transitions have been proven to be extremely weak in the pendular limit. Using this labeling ability, simulated spectra can be easily assigned in terms of  $v_x$ ,  $v_y$ , and  $m$ .

## B. Population transfer

Distribution of the ground-state population has to be known for a spectrum simulation. Because the ground-state population depends not only on the molecular properties but also on experimental methods and conditions, it is difficult to develop a general method to estimate it. In most experiments, including the present study, a molecular sample is prepared with a supersonic expansion in a field-free region and goes into a uniform-field region between two parallel electrodes. In the field-free region, the ground-state distribution is regarded as a Boltzmann distribution at a certain rotational temperature. In the uniform-field region, however, the state distribution is not so simple. As the molecule approaches the electrodes, rotational energy levels change drastically and a lot of level crossings take place. In the asymmetric-top case, the absence of rotational symmetry around a molecular principal axis produces a large number of avoided crossings. Considering the effect of hyperfine interactions, the avoided crossings occur even in the linear-rotor and symmetric-top cases. Therefore, a precise estimation of the state distribution requires examinations of nonadiabatic transitions at each avoided crossing until the molecules reach the uniform-field region. This examination demands extraordinary efforts, in particular, for the case of large molecules. Since energy levels of large molecules are congested, a vast number of level crossings take place in the approach to the electrodes. Furthermore, the ground-state population spreads up to high  $j$  states even in a jet-cooled condition. Thus, the number of states is too large to inspect each level crossing precisely. Therefore, some population model should be introduced in order to calculate ground-state distributions. This problem has been discussed in relation to manipulations of molecular orientations by the brute force technique. Loison *et al.*<sup>38</sup> studied the orientation process of ICl, including the effects of hyperfine interactions, and estimated the character (adiabatic or nonadiabatic) of the population transfer at several types of avoided crossings. Some groups also examined the avoided crossings for the case of asymmetric-top molecules and calculated the molecular orientation using several types of population transfer models.<sup>7,11</sup> In this section, we describe a population transfer model that is similar to the models adopted in the previous studies and suitable for spectral simulation with the approximate method developed in this paper.

For considerations of the population model, it is important to examine the nature of the crossings. The state crossings are roughly classified into the following two categories:

$m$ -type crossing, which is an avoided crossing between different  $m$  states and  $v$ -type crossing, which is an avoided crossing between states with different  $v_{x,y}$  and the same  $m$ .  $m$  is a good quantum number in the uniform-field region, where the space-fixed  $Z$  axis is set along the electric-field vector. However, before the molecule arrives at the uniform-field region, the cylindrical symmetry around the  $Z$  axis is broken. Thus,  $m$  may not be a good quantum number in the region where level crossings take place, and  $m$ -type crossing will originate from the symmetry breaking. If the molecule passes through the  $m$ -type crossing adiabatically, the state character about  $m$  switches to each other. In order to distinguish whether the level crossings take place adiabatically or nonadiabatically, it is useful to introduce the criterion for adiabatic passage  $\eta$ ,<sup>39</sup>

$$\eta = \frac{2\pi V_{12}^2}{\hbar u \Delta F}, \quad (9)$$

where  $V_{12}$  is the half of the energy difference between two adiabatic levels at a point of the avoided crossing,  $u$  is the velocity of molecules, and  $\Delta F$  is a difference of the slopes between the two diabatic levels. In the  $m$ -type crossing, the maximum value of  $V_{12}$  is approximated as an interaction between the electric-quadrupole moment of molecules and the gradient of electric fields. Then,  $V_{12}$  is at most in the order of  $10^{-6}$  cm<sup>-1</sup>. Applying the typical values of  $u \sim 10^5$  cm/s and  $\Delta F \sim 10^1 - 10^{-1}$  cm<sup>-2</sup>,  $\eta$  is calculated to be  $< 10^{-5}$ , and the behavior is fully diabatic. Therefore,  $m$  is a good quantum number even in the region when symmetry around the  $Z$  axis is broken, and the symmetries of the groups discussed in Ref. 30 approximately holds throughout the passage. On the other hand,  $v$ -type crossing is difficult to evaluate. On the symmetry considerations, energy levels of the same irreducible representation should avoid each other. However, the strength of mixing varies largely from one crossing to another, so that  $V_{12}$  is hard to estimate. In this study,  $v$ -type crossing is assumed to be fully adiabatic. While this assumption may give some uncertainty, serious errors would not arise on the grounds that Kong and Bulthuis<sup>11</sup> calculated ground-state distributions in adiabatic and nonadiabatic population models and concluded that the two distributions are not so different from one another. Therefore, the adiabatic population transfer model, in which  $m$ -type crossing is fully diabatic and  $v$ -type crossing is fully adiabatic, is used for calculating the ground-state distribution. Actual calculations are carried out as follows: energy levels in the field-free condition are first calculated for each symmetry in order to estimate the population factor of the Boltzmann distribution. Second, energy levels of the same symmetry as the field-free computation are calculated in a pendular condition. Then, the population in the  $n$ th pendular level is determined as the population of the  $n$ th level under the field-free condition of the same symmetry, where energy levels in each condition are arranged in an ascending order.

## IV. RESULTS AND DISCUSSION

The  $S_1 - S_0$  transition dipole in 9CNA is parallel to the  $b$  axis, similar to the permanent dipole. The molecular axes are

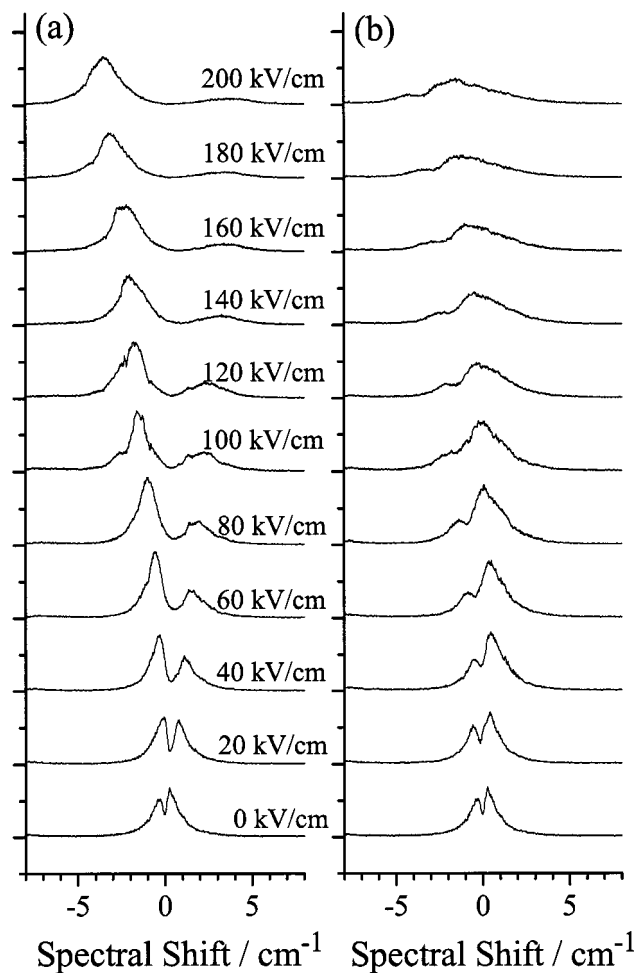


FIG. 4. Fluorescence excitation spectra of the  $S_1-S_0$  origin band of 9CNA under field strengths up to 200 kV/cm with 20 kV/cm increments. Spectral shifts are relative to the field-free origin at 382.13 nm. The polarization of the excitation laser is set (a) parallel and (b) perpendicular to the external field.

chosen as  $(x, y, z) = (c, a, b)$ , and, thus, the electronic transition is categorized as the  $\mu_z$  type.<sup>30</sup> By using the molecular parameters derived from the previous studies,<sup>35,36</sup>  $\lambda$  in  $S_0$  is calculated to be  $\approx 0.054$  under the 200-kV/cm field. Therefore, the pendular condition is sufficiently satisfied.

The fluorescence excitation spectra of the  $S_1-S_0$  origin band of 9CNA were measured under various electric fields (from 0 to 200-kV/cm field strengths by 20-kV/cm step) in two configurations where the polarizations of the laser light were parallel and perpendicular to the static electric field, namely, the  $\mu_z$  and  $\mu_x$  configurations, respectively. The spectra are depicted in Fig. 4. The band shape changed drastically as the field strength increased. The spectra taken with the  $\mu_z$  configuration are shown in Fig. 4(a). As the field strength became larger, the origin band was split into two parts, redshifted and blueshifted bands. The redshifted band was stronger than the blueshifted one, and this tendency became substantial with the field increase. Both of the bands were broadened as the external field was increased. Their peak shifts were approximately proportional to the field strength with the similar absolute value for the increments. Figure 4(b) shows the spectra measured in the  $\mu_x$  configu-

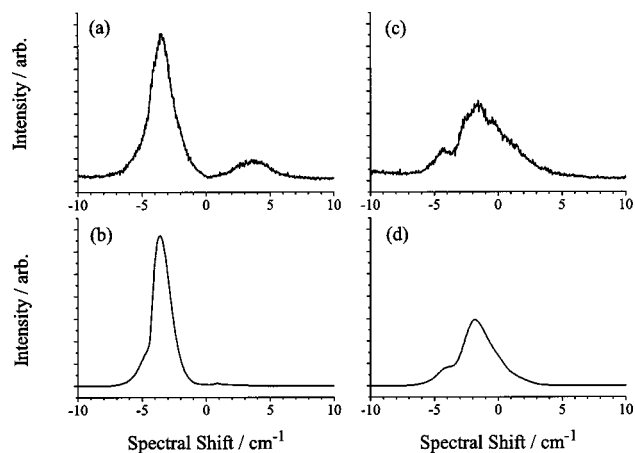


FIG. 5. LIF spectra under the dc electric field of 200 kV/cm. (a) Experimental and (b) simulated spectra in the  $\mu_z$  configuration, and (c) experimental and (d) simulated spectra in the  $\mu_x$  configuration. The parameters used in the calculations are described in the text.

ration. As the applied field increased, the spectrum manifested band broadening. In each spectrum, the band consisted of two elements, a strong band at the higher energy and a weak band at the lower energy. These bands did not show prominent shift.

The observed spectra are analyzed using the approximate method for spectral simulations, which have been described in Sec. III. In the simulations, values for  $\mu$  in  $S_0$  and the rotational constants in  $S_0$  and  $S_1$  are taken from Refs. 35 and 36. The adiabatic population transfer model presented in Sec. III B is adopted for the calculation of the ground-state distribution. From the rotational contour analysis at the 0-kV/cm field, the rotational temperature in the field-free region is determined to be 10 K. We have attempted several calculations with various values for  $\mu$  in  $S_1$ , and the spectra simulated with  $\mu = 5.7$  D best reproduce the experimental spectra. The results are shown in Fig. 5, where the basis size is  $(j_{\max}, v_{\max}) = (200, 40)$ . The gross features of the calculated spectra, such as shapes, positions, and intensity ratio of  $\mu_z$  to  $\mu_x$ , agree reasonably with the observed spectra except for the blueshifted peak in the  $\mu_z$  configuration. Considering the  $\pm 3\%$  accuracy of the field and the laser resolution of  $0.2 \text{ cm}^{-1}$ , the value of  $\mu$  in  $S_1$  is bracketed to be  $5.7 \pm 0.1$  D.

Since the state assignment in terms of the pendular-state quantum numbers,  $(v_x, v_y, m)$ , is available in the present simulations, the spectra of 9CNA can be examined in more details by sorting out the transitions according to the  $\Delta v_{x,y}$  values. Firstly, the spectrum of the  $\mu_z$  configuration is discussed. Since this transition is categorized as the  $\mu_{zz}$  configuration, major contributions to a spectrum are  $(v'_x = v''_x, v'_y = v''_y, m' = m'')$  transitions, where double and single primes denote the ground and the excited states, respectively. Then, the expectation values of the transition energy  $\Delta E$  are represented by<sup>30</sup>

$$\begin{aligned} \Delta E = & -\Delta\mu\epsilon + (v'_x - v''_x)(v''_x + 1/2) \\ & + (v'_y - v''_y)(v''_y + 1/2), \end{aligned} \quad (10)$$

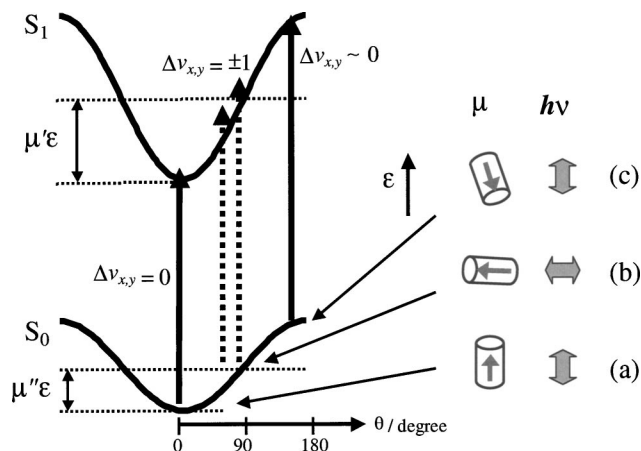


FIG. 6. Schematic diagram for pendular-state spectra of 9CNA. Cartoons denoted as (a), (b), and (c) represent the averaged molecular orientations in states with low, medium, and high values of  $v_{x,y}$ , respectively. Solid and broken arrows indicate strongly allowed transitions for the  $\mu_z$  and  $\mu_x$  configurations, respectively. Because the interaction potential in  $S_1$  is deeper than that in  $S_0$ , transitions from the states of (a) are redshifted from the field-free position, whereas those from (c) are blueshifted. Transitions from (b) do not shift so much.

where  $v_x = \sqrt{2A\mu\epsilon}$  and  $v_y = \sqrt{2C\mu\epsilon}$ . As schematically depicted in Fig. 6, the redshift of the strong peak corresponds to the zero-point shift, which is expressed as  $-\Delta\mu\epsilon$  with  $\Delta\mu = \mu(S_1) - \mu(S_0)$ . At the static field of 200 kV/cm, the observed shift is  $\approx 3.6 \text{ cm}^{-1}$ , which corresponds to  $\Delta\mu = 1.1 \text{ D}$ . This is roughly consistent with the result from the simulation,  $\Delta\mu = 1.3 \pm 0.1 \text{ D}$ . By using this value,  $\lambda$  in  $S_1$  is calculated to be  $\approx 0.047$ . The fundamental frequencies of the pendular vibrations in the excited state are estimated as  $\nu'_x \approx 1.1 \text{ cm}^{-1}$  and  $\nu'_y \approx 0.63 \text{ cm}^{-1}$ . These values are slightly larger than the corresponding values in the ground state,  $\nu''_x \approx 1.0 \text{ cm}^{-1}$  and  $\nu''_y \approx 0.55 \text{ cm}^{-1}$ . The difference of the fundamental frequencies between the ground and excited states makes the transitions with different  $v''_{x,y}$  split apart [see Eq. (10)]. Since our laser resolution is far insufficient to resolve each of the transitions and the spectrum is composed of vast numbers of individual transitions with spread ground-state distributions, the band contour is determined as a convolution of many transitions of different types. In Fig. 7, the spectrum is decomposed into the contributions from the transitions with different pendular-state selection rules. It is apparent that most of the stronger redshifted peak originates in the transitions with  $\Delta v_x = 0$  and  $\Delta v_y = 0$ , which possess the largest oscillator strength in the case that the dipoles of the ground and the excited states are similar to one another. The small shoulder at the low-frequency side of the peak is due to the transitions with  $\Delta v_{x,y} = -2$ , induced by the difference between the dipoles and the higher-order terms in the power-series expansion of the dipole operator with  $\lambda$ . It is interesting that the transitions with  $\Delta v_{x,y} = +2$  are much weaker than those with  $\Delta v_{x,y} = -2$ , even though the absolute changes in  $v_{x,y}$  are the same. Note that transitions with odd  $\Delta v_{x,y}$  are forbidden by symmetry for the  $\mu_z$  type transition.<sup>30</sup> Thus, the description with the pendular-state selection rules presented in Ref. 30 holds well for the spectrum of the large asymmetric-top molecule, 9CNA. The gross feature of the

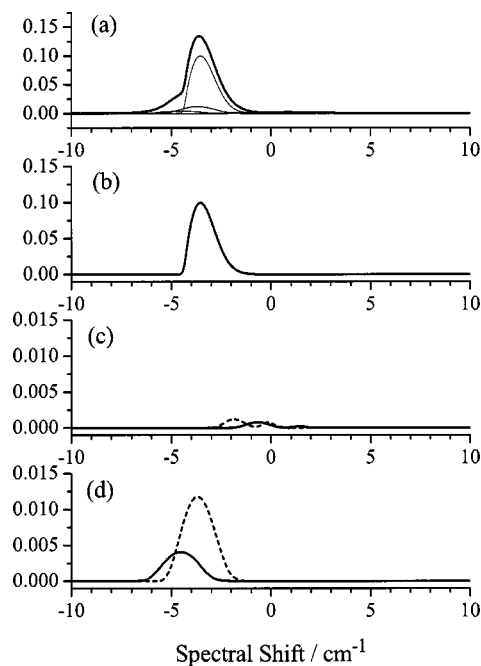


FIG. 7. Simulated spectra in the  $\mu_z$  configuration at 200 kV/cm. (a) Spectrum including all the transitions (thick line) and contributions from each of the transitions with different  $\Delta v_x$  and  $\Delta v_y$  depicted in the lower panels (b)–(d) (thin lines). (b) Transitions with  $\Delta v_x = 0$  and  $\Delta v_y = 0$ . (c) Transitions with  $\Delta v_x = +2$  and  $\Delta v_y = 0$  (solid line) and those with  $\Delta v_x = 0$  and  $\Delta v_y = +2$  (broken line). (d) Transitions with  $\Delta v_x = -2$  and  $\Delta v_y = 0$  (solid line) and those with  $\Delta v_x = 0$  and  $\Delta v_y = -2$  (broken line). It is noted that the vertical scales of (c) and (d) are expanded by a factor of ten relative to those of (a) and (b).

spectra in the  $\mu_x$  configuration can be explained as well by the spectral simulations in which the spectrum is decomposed into the contributions from the different pendular-states selection rules, as shown in Fig. 8. The main part of the larger peak is due to transitions with  $\Delta v_{x,y} = +1$ , while the weaker one in the lower-frequency side originates in the transitions with  $\Delta v_{x,y} = -1$ . These transitions possess the largest oscillator strength in the configuration. The main peak exhibits a tail in the high-frequency side and this part corresponds to transitions with  $\Delta(v_x + v_y) = +3$ , which originate in the difference between the dipoles and the higher-order terms in  $\lambda$ .

The simulated spectrum cannot reproduce the weaker peak exhibiting a blueshift in the  $\mu_z$  configuration. This peak is probably due to transitions with quite high  $v''_{x,y}$  values, as schematically explained in Fig. 6. States with high  $v''_{x,y}$  will have sizable probability around  $\theta = 180^\circ$  because the dipole-field interaction potential has a barrier at  $\theta = 180^\circ$  and wave functions of highly excited states have a larger distribution around the potential wall. Thus, molecules distributed in such states show the preference for the dipoles anti-parallel to the field. Such a spatial orientation of molecules, denoted as (c) in Fig. 6, is favorable to the absorption of light in the  $\mu_z$  configuration because the transition moment is (anti)parallel to the permanent dipole in 9CNA. Thus, the transitions from high  $v''_{x,y}$  states possess large oscillator strengths, similar to those from states near the bottom of the potential, denoted as (a) in Fig. 6. Transitions in this configuration

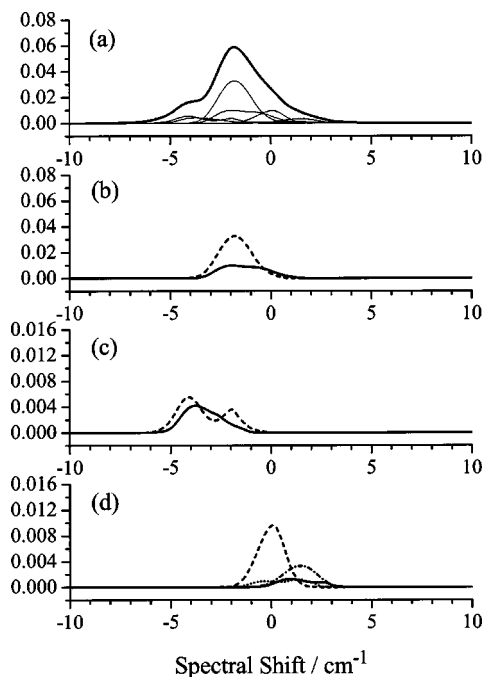


FIG. 8. Simulated spectra in the  $\mu_x$  configuration at 200 kV/cm. (a) Spectrum including all the transitions (thick line) and contributions from each of the transitions with different  $\Delta v_x$  and  $\Delta v_y$  depicted in the lower panels (b)–(d) (thin lines). (b) Transitions with  $\Delta v_x = +1$  and  $\Delta v_y = 0$  (solid line) and those with  $\Delta v_x = 0$  and  $\Delta v_y = +1$  (broken line). (c) Transitions with  $\Delta v_x = -1$  and  $\Delta v_y = 0$  (solid line) and those with  $\Delta v_x = 0$  and  $\Delta v_y = -1$  (broken line). (d) Transitions with  $\Delta v_x = +3$  and  $\Delta v_y = 0$  (solid line),  $\Delta v_x = 0$  and  $\Delta v_y = +3$  (broken line),  $\Delta v_x = +1$  and  $\Delta v_y = +2$  (dotted line), and  $\Delta v_x = +2$  and  $\Delta v_y = +1$  (chain line). It is noted that the vertical scales of (c) and (d) are expanded by a factor of five relative to those of (a) and (b).

obey the pendular-state selection rules that  $\Delta v_{x,y}$  should be small even numbers. The fundamental frequencies for the pendular vibrations are larger in the excited states than in the ground states. Thus, the transitions from high  $v''_{x,y}$  states appear with a large blueshift from the main peak. In the  $\mu_x$  configuration, on the other hand, molecules with their dipoles perpendicular to the external field preferentially absorb the light. Thus, the spectrum is composed of transitions from the states with medium  $v''_{x,y}$  values, of which the probability amplitude has a large value around  $\approx 90^\circ$  [(b) in Fig. 6]. Failure in the reproduction of the blueshifted peak in the  $\mu_z$  configuration probably originates from the deficiencies in the method for spectral simulations as below. First, the size of the basis set may be insufficient for properly describing the highly excited states. Another possibility is a discrepancy in the ground-state distribution from the population transfer model adopted herein. The present model assumes that the population of the levels is adiabatically transferred at all  $v$ -type avoided crossings. If some nonadiabaticities exist, populations of lower-energy states in the field-free region are partly transferred to the higher-energy states in the uniform-field region. As a result, the calculated populations at highly vibrating states should be underestimated relative to the real distribution affected by nonadiabatic population transfers.

## V. CONCLUSION

The present study has realized the pendular condition for an asymmetric-top molecule much closer to the strong field

limit than ever has been reported.<sup>3,8,10</sup> The achievement was owing to the application of uniform electric fields up to 200 kV/cm without serious electric discharges by utilizing two parallel Rogowski-type electrodes in the fluorescence excitation measurements, as well as, the large permanent dipole moment and small rotational constants of 9-cyanoanthracene studied herein. The observed pendular-state spectrum pertinent to the  $S_1-S_0$  origin band was so distinct from that in the field-free condition, and the spectral shift for the major peak reached to  $\approx 3.6 \text{ cm}^{-1}$  at the maximum field strength for the excitation configuration where the laser polarization direction was set parallel to the external field. An approximate method to simulate pendular-state spectra of large asymmetric-top molecules has been developed and employed to show that the observed spectra are well ascribed on the basis of the pendular-limit representation on energy levels and spectra, which has been recently derived by the present authors.<sup>30</sup> In particular, each part of the pendular spectra has been classified into transitions with different selection rules and degrees of vibrational excitations. Thus, the present results indicate the possibility of precise control in orientational distribution of molecules by selecting the probed region in a pendular spectrum. For example, molecular orientation in an electronically excited state can be improved substantially by the laser excitation of molecules only in low pendular-vibration states.

## ACKNOWLEDGMENTS

The authors thank Professor O. Kajimoto for his encouragement and support throughout the study. The high-voltage electrodes were constructed by the Instrumental Development Center of the Institute for Molecular Science. The present work has been partly supported by Grants-in-Aid (Grant Nos. 14340180, 15035206, and 16032206) from MEXT of Japan and the grants from JAERI and Sumitomo Science Foundation.

- <sup>1</sup>H. J. Loesch and A. Remscheid, *J. Chem. Phys.* **93**, 4779 (1990).
- <sup>2</sup>B. Friedrich and D. R. Herschbach, *Z. Phys. D: At., Mol. Clusters* **18**, 153 (1991).
- <sup>3</sup>D. T. Moore, L. Oudejans, and R. E. Miller, *J. Chem. Phys.* **110**, 197 (1999).
- <sup>4</sup>H. J. Loesch and A. Remscheid, *J. Phys. Chem.* **95**, 8194 (1991).
- <sup>5</sup>B. Friedrich, D. P. Pullman, and D. R. Herschbach, *J. Phys. Chem.* **95**, 8118 (1991).
- <sup>6</sup>B. Friedrich, D. R. Herschbach, J. M. Rost, H. G. Rubahn, M. Renger, and M. Verbeek, *J. Chem. Soc., Faraday Trans.* **89**, 1539 (1993).
- <sup>7</sup>J. Bulthuis, J. Möller, and H. J. Loesch, *J. Phys. Chem. A* **101**, 7684 (1997).
- <sup>8</sup>H. Li, K. J. Franks, R. J. Hanson, and W. Kong, *J. Phys. Chem. A* **102**, 8084 (1998).
- <sup>9</sup>B. Friedrich and D. Herschbach, *J. Chem. Phys.* **111**, 6157 (1999).
- <sup>10</sup>K. J. Franks, H. Li, and W. Kong, *J. Chem. Phys.* **110**, 11779 (1999).
- <sup>11</sup>W. Kong and J. Bulthuis, *J. Phys. Chem. A* **104**, 1055 (2000).
- <sup>12</sup>B. Friedrich and D. Herschbach, *Phys. Chem. Chem. Phys.* **2**, 419 (2000).
- <sup>13</sup>R. J. Bemish, M. C. Chan, and R. E. Miller, *Chem. Phys. Lett.* **251**, 182 (1996).
- <sup>14</sup>G. Bazalgette, R. White, G. Tréneç, E. Audouard, M. Büchner, and J. Vigué, *J. Phys. Chem. A* **102**, 1098 (1998).
- <sup>15</sup>L. Oudejans and R. E. Miller, *J. Chem. Phys.* **109**, 3474 (1998).
- <sup>16</sup>L. Oudejans and R. E. Miller, *J. Phys. Chem.* **99**, 13670 (1995).
- <sup>17</sup>L. Oudejans and R. E. Miller, *J. Phys. Chem. A* **101**, 7582 (1997).
- <sup>18</sup>A. Slenczka, B. Friedrich, and D. Herschbach, *Chem. Phys. Lett.* **224**, 238 (1994).

- <sup>19</sup>A. Durand, J. C. Loison, and J. Vigué, *J. Chem. Phys.* **101**, 3514 (1994).  
<sup>20</sup>A. Durand, J. C. Loison, and J. Vigué, *J. Chem. Phys.* **106**, 477 (1997).  
<sup>21</sup>R. Kanya and Y. Ohshima, *Chem. Phys. Lett.* **370**, 211 (2003).  
<sup>22</sup>K. J. Castle and W. Kong, *J. Chem. Phys.* **112**, 10156 (2000).  
<sup>23</sup>K. J. Castle, J. Abbott, X. Peng, and W. Kong, *J. Chem. Phys.* **113**, 1415 (2000).  
<sup>24</sup>K. J. Castle, J. E. Abbott, X. Peng, and W. Kong, *J. Phys. Chem. A* **104**, 10419 (2000).  
<sup>25</sup>K. Nauta and R. E. Miller, *Science* **283**, 1895 (1999).  
<sup>26</sup>K. Nauta and R. E. Miller, *J. Chem. Phys.* **111**, 3426 (1999).  
<sup>27</sup>K. Nauta, D. T. Moore, and R. E. Miller, *Faraday Discuss.* **113**, 261 (1999).  
<sup>28</sup>K. Nauta and R. E. Miller, *Phys. Rev. Lett.* **82**, 4480 (1999).  
<sup>29</sup>K. Nauta and R. E. Miller, *J. Chem. Phys.* **117**, 4846 (2002).  
<sup>30</sup>R. Kanya and Y. Ohshima, *Phys. Rev. A* **70**, 013403 (2004).  
<sup>31</sup>S. Heitz, D. Weidauer, and A. Hese, *Chem. Phys. Lett.* **176**, 55 (1991).  
<sup>32</sup>S. Heitz, R. Lampka, D. Weidauer, and A. Hese, *J. Chem. Phys.* **94**, 2532 (1991).  
<sup>33</sup>S. Heitz, D. Weidauer, B. Rosenow, and A. Hese, *J. Chem. Phys.* **96**, 976 (1992).  
<sup>34</sup>M. Okruss, R. Müller, and A. Hese, *J. Chem. Phys.* **110**, 10393 (1999).  
<sup>35</sup>K. Egashira, Y. Ohshima, and O. Kajimoto, *J. Phys. Chem. A* **105**, 1131 (2001).  
<sup>36</sup>Y. Ohshima, R. Kanya, Y. Sumiyoshi, and Y. Endo, *J. Mol. Spectrosc.* **223**, 148 (2004).  
<sup>37</sup>A. Amirav, C. Horwitz, and J. Jortner, *J. Chem. Phys.* **88**, 3092 (1988).  
<sup>38</sup>J. C. Loison, A. Durand, G. Bazalgette, R. White, E. Audouard, and J. Vigué, *J. Phys. Chem.* **99**, 13591 (1995).  
<sup>39</sup>C. Zener, *Proc. R. Soc. London, Ser. A* **137**, 696 (1932).